# Method of Moments Analysis of Arbitrary Structures in Shielded Layered Media

James C. Rautio, *Life Fellow, IEEE*, Matthew A. Thelen, *Member, IEEE*

***Abstract*— Method of moments analysis of planar multilayer circuits typically assumes that conductors are infinitely thin and only surface currents need be modeled. Modern fabrication techniques, especially for high-frequency integrated circuits, can easily create structures that require modeling volume current. We present here a complete *volume current*-based method of moments analysis of arbitrary structures embedded in shielded multilayer media. The volume rooftop, uniform via, and tapered via basis functions that we present are key for such an analysis. The embedding layered media is not meshed as it is automatically included in the Green's function. The required integrations (in six dimensions) of the Green's function have been evaluated analytically with full results presented as a two-dimensional infinite summation that is rapidly evaluated to full precision using the FFT algorithm. Planar circuits using thick metal are typically analyzed to high accuracy one to three orders of magnitude faster due to reduced subsection count.**

***Index Terms*— Electromagnetic (EM), GaAs, Galerkin, integrated circuit, method of moments, planar, radio frequency integrated circuit (RFIC), rooftop, silicon, thick conductor.**

## I. Introduction

METHOD of moments [1] as applied to electromagnetic (EM) analysis of planar circuits has been widely implemented for both unshielded [2] and shielded [3] planar circuits in layered media by assuming 2-D, infinitely thin sheets of current are sufficient to model actual planar microwave circuits. However, modern circuit fabrication techniques, especially for Si and GaAs microwave integrated circuits, can realize planar microwave components with conductors that are thick compared to line widths or line-to-line gaps. A typical example is shown in [4, Fig. 1]. Accurate EM analysis can be difficult.

One fully validated solution is to use a multisheet model of thickness [5]. This model converges to the correct answer as the mesh size is reduced and the number of sheets is increased. In fact, one of the validation strategies we use is to check that the multisheet model converges to the same answer as that obtained by the theory described in this article. However, as is demonstrated by measured analysis times, the multisheet model can require excessive compute resources for complex circuits that use thick metal, while the approach described in this article provides essentially the same answer much faster.

Manuscript received July 20, 2020; revised September 3, 2020; accepted September 19, 2020. This article is an expanded version from IMS2020, Virtual (moved from Los Angeles, CA), July–August 2020. *(Corresponding author: James C. Rautio.)*

The authors are with Sonnet Software, Inc., Syracuse, NY 13212 USA (e-mail: rautio@sonnetsoftware.com).

Color versions of one or more of the figures in this article are available online at http://ieeexplore.ieee.org.

Digital Object Identifier 10.1109/TMTT.2020.3026376

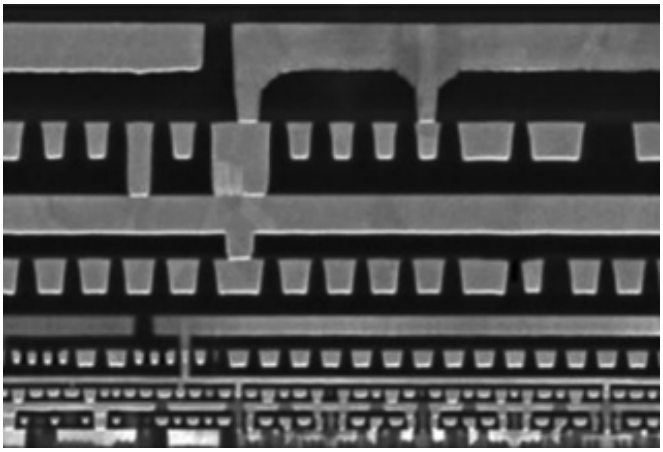

Fig. 1. Scanning electron microscope (SEM) image of a cross section of a SiRFIC using the Intel's 14-nm process with 52-nm minimum pitch. Line thickness (vertical) can be larger than the linewidth (horizontal) and larger than the gap between lines as well, creating an extreme EM analysis problem for large circuits. From [4].

Volume basis functions have been used in method of moments in the past. For example, Polychronopoulos and Uzunoglu [6] solved the 2-D dielectric waveguide problem, representing fields in the entire volume of the problem using entire domain basis functions. Of course, there are a wide variety of additional techniques, such as finite element, finite difference time domain (FDTD), and transmission line method (TLM), which mesh the entire volume and are not detailed here.

Equivalent fictious electric and magnetic surface currents (e.g., polarization currents) can also be used in method of moments to model 3-D structures, as well as a combination of surface and volume polarization currents. For example, Gholami *et al.* [7] used Rao–Wilton–Glisson (RWG) surface current basis functions [8] combined with volume tetrahedra basis functions to model scattering in free space and in layered, unshielded media, i.e., the layers extend laterally to infinity. The theory described in this article could be applied to a similar approach and may be the subject of future research.

In this article, we model the actual volume current using volume subsections. Use of a surface current "rooftop" subsection [8] (i.e., basis function) has been widespread. This has been extended to volume rooftop subsections [9]. Modeling horizontal volume currents using volume rooftop subsections in a multilayer circuit also requires a "via" subsection that allows current to flow vertically from one layer to another [10].

Two types of via subsections are required. First, a via that has uniform current flowing along its vertical length, and

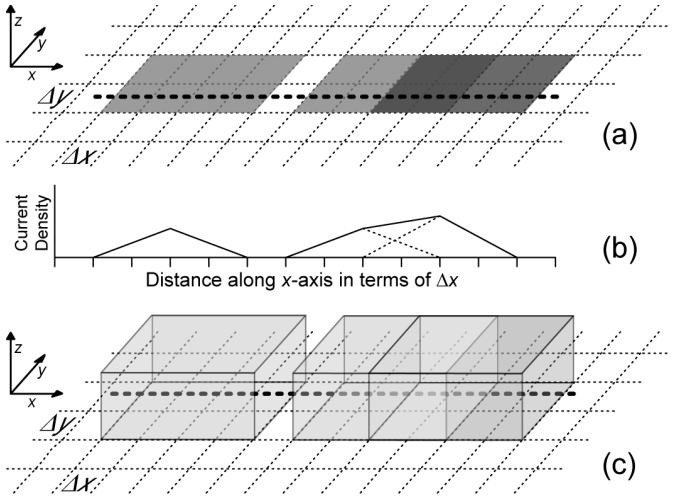


Fig. 2. Infinitely thin surface current-based rooftop subsections occupy a rectangular footprint (a). Current (b) along the thick dashed line in (a) shows how two overlapping subsections (right) add to give a piecewise linear representation of the current. Volume current-based rooftops occupy a rectangular prism (c), but two overlapping subsections (right) also yield a piecewise linear representation of the volume current (b). From [9].

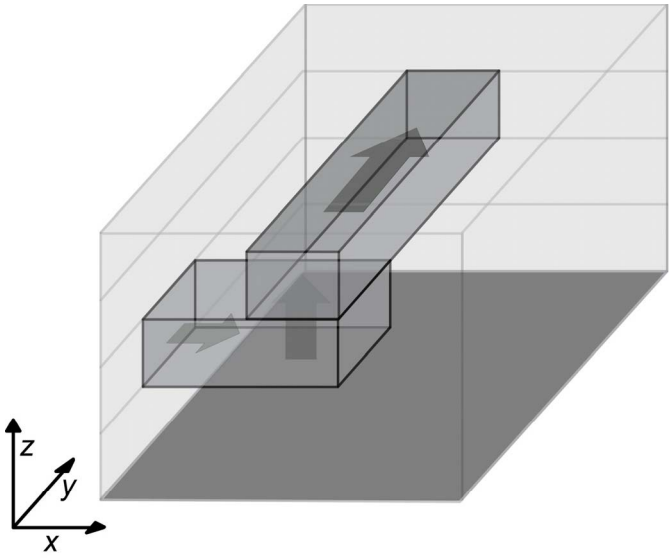


Fig. 3. Illustrative multilayer shielded planar circuit requires $z$-directed current to make the electrical connection from the right end of the lower conductor to the near end of the upper conductor. Because the conductors are thick, both horizontal and vertical currents (arrows) are best modeled by volume current basis functions.

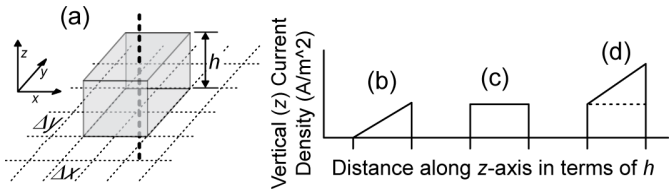


Fig. 4. Single, dimensioned, via block (a) and the variation in $z$-directed current along the z-direction for an up tapered via (b), a uniform via (c), and for a block that contains both a tapered and uniform via (d). Current for all vias is constant across a given $x$-$y$ cross section.

second, a via whose current tapers linearly from zero at the bottom to maximum at the top, i.e., a "tapered via." Green's functions and full method of moments reaction integral results are provided for both types of via in this article.

These results, combined with results for horizontal volume current rooftop subsections [9], which are summarized here, enable a complete *volume current*-based method of moments analysis of arbitrary structures embedded in multilayered planar media. This analysis approach has been implemented in a software package [11] that is useful for design of planar circuits that use thick conductors, a situation now becoming common for silicon radio frequency integrated circuits (SiRFICs). This article is an expanded version of [12].

Note that this method meshes only the structure that is embedded in the layered media. It does not mesh the layered media as that is automatically and exactly included in the Green's function. This reduces the size of the numerical problem substantially as compared to techniques that require meshing the entire volume.

## II. Volume Subsection Types

Fig. 2(a) shows the original infinitely thin, surface current-based rooftop subsections. The $x$-directed surface current density along the thick dashed line is shown in Fig. 2(b), in A/m. The right side of Fig. 2(a) and (b) shows how overlapping infinitely thin rooftop basis functions provide a piecewise linear representation of current flow in the direction of current flow. An arbitrary, infinitely thin circuit is meshed twice, once into overlapping $x$-directed rooftops and a second time into $y$-directed rooftops.

The surface rooftops of Fig. 2(a) expand vertically to become volume rooftops with volume current (A/m$^2$) in Fig. 2(c). Just as with surface rooftops, overlapping volume rooftops, Fig. 2(c) (right), result in a piecewise linear representation of the actual volume current. And again, an arbitrary (thick) planar structure is meshed twice, once for $x$-directed volume rooftops and a second time for $y$-directed volume rooftops. Horizontal ($x$- and $y$-directed) volume rooftops are then used to mesh horizontal portions of the circuit metal in Fig. 3. See [9] for details.

This leaves $z$-directed current. Consider the region of transition of the circuit in Fig. 3 where the two lines overlap and touch. This region consists of two "blocks." The bottom block envelops the right end of the bottom line. The top block envelops the near end of the top line. It is in these two regions that vertical ($z$-directed) current flows. Fig. 4(a) shows a single block including dimensional nomenclature.

Considering a block enveloping the right end of the bottom line in Fig. 3, the vertical current must be zero on the bottom surface. Only horizontal current can flow there. At the top surface of the bottom block (where the bottom and top blocks touch), we have maximum vertical current. This is where all the previously horizontal current from the bottom line is now flowing vertically to connect with the near end of the top line.

Thus, in order to model the vertical current in the bottom block, we need a via subsection with zero current at the bottom and maximum current at the top, i.e., a tapered via [10], [12]. We also refer to this as an "up via" as it is used to transition current upward from a horizontal volume rooftop. In this work, if via type is not specified, a tapered via is always assumed to

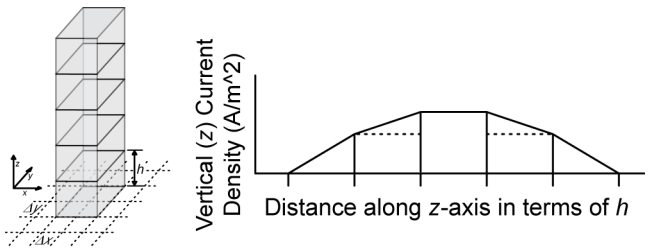


Fig. 5. A lengthy (compared to wavelength) via can be accurately modeled by a stack of vias. The density of the $z$-directed current along the z-direction is shown on the right. The bottom block needs only an uptapered via. The top block needs a downtapered via. All other blocks should be filled with both a tapered and a uniform via.

be an up via. Note that the "taper" refers only to the vertical current density variation within the via. The physical shape of a tapered via is a rectangular prism, i.e., a rectangular block, Fig. 4(a).

Consider now the vertical current in the top block, at the near end of the top line. The top surface of the top block must have zero vertical current. All current flow has transitioned to horizontal current flow in the volume rooftops used to model the top line.

The bottom surface of the top block, where it meets the top surface of the bottom block, must have maximum vertical current as all the previously horizontal current is flowing vertically across this surface.

Thus, we need a tapered via that has zero current at the top and maximum current at the bottom in order to model the vertical component of current in this region. We refer to this as a "down via" [10], [12] as it can be used to transition current downward. In fact, a down via positioned on the next layer up from an up via (as is the situation in this example) together form a split vertical volume rooftop subsection that extends vertically across two adjacent dielectric layers.

## III. Via Relations

Fig. 4(a) shows a single dimensioned via block. Fig. 4(b) shows the magnitude of the vertical volume current along the thick dashed line within the via block when a tapered volume up via subsection (i.e., basis function) occupies that block. The current is the same everywhere in any horizontal cross section, and it tapers linearly from zero at the bottom to a maximum at the top, or, assuming the base of the block is at $z = 0$

$$J_z = z/h. \tag{1}$$

Fig. 4(c) illustrates the current distribution on a "uniform via," i.e., a via that has constant current along its entire length.

Fig. 4(d) shows the total vertical current in a block that is occupied by both an up via and a uniform via. If arbitrary and independent magnitudes, or weights, can be assigned to each of the two co-located vias (as is the usual approach in method of moments), then we can model current with any slope at any level. If, as is typical, the weights may be complex (i.e., real and imaginary), a linear phase variation along the length of the via is also modeled.

Such a model is illustrated in Fig. 5 for a via stack, yielding a piecewise linear representation of the current on the via stack. The bottom end of the stack contains only an up via. The top end needs only a down via. All other blocks contain both an up via and a uniform via.

An actual down via is not required. If a block is occupied by both an up via and a uniform via, method of moments assigns a negative weight to the up via when a down via is required. This subtracts the up via current from the uniform via current creating the effect of a down via. Fundamentally, a down via is an up via subtracted from a uniform via. Thus, of the three types of vias: down, uniform, and up; only two should be used in any given volume block as the third is a linear combination of the other two. Placement of all three via types in the same via block results in a singular moment matrix. Here, we consider only the uniform via and up via. If a down via is needed it is formed by subtracting an up via from a uniform via.

As mentioned above, a down via placed directly above an up via effectively forms a vertically oriented volume rooftop basis function that crosses over two dielectric layers. These vias, combined with the horizontal $x$- and $y$-directed volume rooftops are the key elements required for modeling completely arbitrary 3-D structures embedded in shielded multilayered media.

## IV. Field Description

The fields in any given layer are represented as a weighted summation of all TE, TM, $m$, $n$ rectangular waveguide modes with the sidewalls of the box containing the layered media forming the waveguide, Figs. 2 and 3. The embedding dielectric layers are all parallel to the $xy$-plane. For brevity, we use the index $i$ to represent all $m$, $n$, TE, TM modes. The index is not always explicit. After [13], we start with modal normalizing constants

$$N_1 = \sqrt{\frac{2}{ab}}, \quad m = 0,\ n > 0 \tag{2}$$

$$N_1 = \frac{2k_y}{k_c\sqrt{ab}}, \quad m > 0,\ n > 0 \tag{3}$$

$$N_2 = \sqrt{\frac{2}{ab}}, \quad m > 0,\ n = 0 \tag{4}$$

$$N_2 = \frac{2k_x}{k_c\sqrt{ab}}, \quad m > 0,\ n > 0 \tag{5}$$

$$N_3 = \frac{2k_c}{k_z^2\sqrt{ab}}, \quad m > 0,\ n > 0. \tag{6}$$

Following are the usual rectangular waveguide wavenumbers and modal characteristic admittances. Quantities with no subscript denote the constitutive parameters of the subject embedding dielectric layer itself. The modal admittances are those of the standing wave modes and thus differ from the usual admittances by a factor of $j$

$$k_{iz}^2 = k^2 - k_{ic}^2 \tag{7}$$

$$k_{ic}^2 = k_x^2 + k_y^2 = \left(\frac{m\pi}{a}\right)^2 + \left(\frac{n\pi}{b}\right)^2 \tag{8}$$

$$Y_{i\mathrm{TE}} = \frac{k_{iz}}{j\omega\mu} \tag{9}$$

$$Y_{i\mathrm{TM}} = -\frac{j\omega\varepsilon}{k_{iz}}. \tag{10}$$

The possible transverse variations of various fields are represented by

$$g_1(x, y) = \cos(k_x x)\sin(k_y y) \tag{11}$$
$$g_2(x, y) = \sin(k_x y)\cos(k_y x) \tag{12}$$
$$g_3(x, y) = \sin(k_x y)\sin(k_y y). \tag{13}$$

The normalized modal vectors follow. We include a normalized modal vector for $z$-directed TM electric fields, which supplements [13]. TE $z$-directed magnetic fields are not needed for this work

$$\boldsymbol{e}_{\text{it}}^{TE} = N_1 g_1 \boldsymbol{u}_x - N_2 g_2 \boldsymbol{u}_y \tag{14}$$
$$\boldsymbol{h}_{\text{it}}^{TE} = N_2 g_2 \boldsymbol{u}_x + N_1 g_1 \boldsymbol{u}_y \tag{15}$$
$$\boldsymbol{e}_{\text{it}}^{\text{TM}} = N_2 g_1 \boldsymbol{u}_x + N_1 g_2 \boldsymbol{u}_y \tag{16}$$
$$\boldsymbol{e}_{iz}^{\text{TM}} = k_z N_3 g_3 \boldsymbol{u}_z \tag{17}$$
$$\boldsymbol{h}_{\text{it}}^{\text{TM}} = -N_1 g_2 \boldsymbol{u}_x + N_2 g_1 \boldsymbol{u}_{y.} \tag{18}$$

The actual fields for the $i$th normalized mode in the subject layer are

$$\boldsymbol{E}_{\text{it}} = \{F_i \sin(k_{iz}z) + G_i \cos(k_{iz}z)\}\boldsymbol{e}_{\text{it}} \tag{19}$$
$$\boldsymbol{E}_{iz}^{\text{TM}} = -\{F_i \cos(k_{iz}z) - G_i \sin(k_{iz}z)\}\boldsymbol{e}_{iz}^{\text{TM}} \tag{20}$$
$$\boldsymbol{H}_{\text{it}} = -Y_i\{F_i \cos(k_{iz}z) - G_i \sin(k_{iz}z)\}\boldsymbol{h}_{\text{it}}. \tag{21}$$

In the usual manner, $F_i$ and $G_i$ are determined by matching boundary conditions at the top and bottom of the layer. In some cases, derivations are simplified by a change of variables from $z$ to (h-z). In this case, also change the sign of (20) and (21).

## V. Green's Functions

The Green's function for unshielded (i.e., either no or only one conducting bounding wall) layered media is given in [2] where it is suggested that the shielded layered Green's function can be determined by means of images. This approach was not attempted. No other source to the author's knowledge gives a full treatment of the complete shielded layered Green's function in terms of rectangular waveguide modes, as is required for this work. Thus, it is derived, apparently for the first time, below.

The transverse portion of the full dyadic Green's function is derived by assuming a two layer medium where both layers have the same dielectric properties. The layer thicknesses are $z'$ and $(h-z')$. Modal amplitudes are set to meet the discontinuity in tangential magnetic field due to an infinitesimal dipole located at $(x', y', z')$. The transverse electric field at $(x, y, z)$, from [9], is

$$\boldsymbol{G}_{tt} = -\sum_i \frac{g_T(z)g_B(z')\left[\boldsymbol{u}_S \cdot \boldsymbol{e}_{\text{it}}(x', y')\right]}{Y_i D}\boldsymbol{e}_{\text{it}}(x, y), \quad z \geq z' \tag{22}$$

$$\boldsymbol{G}_{tt} = -\sum_i \frac{g_T(z')g_B(z)\left[\boldsymbol{u}_S \cdot \boldsymbol{e}_{\text{it}}(x', y')\right]}{Y_i D}\boldsymbol{e}_{\text{it}}(x, y), \quad z \leq z' \tag{23}$$

$$g_B(u) = \sin(k_{iz}u) + r_{iB}\cos(k_{iz}u) \tag{24}$$
$$g_T(u) = \sin(k_{iz}(h-u)) + r_{iT}\cos(k_{iz}(h-u)) \tag{25}$$
$$D = (1 - r_{iB}r_{iT})\sin(k_{iz}h) + (r_{iT} + r_{iB})cos(k_{iz}h) \tag{26}$$
$$= g_B(h) + r_{iT}g_{B2}(h) = g_T(0) + r_{iB}g_{T2}(0). \tag{27}$$

Equations (30) and (31) define $g_{B2}$ and $g_{T2}$. The $\boldsymbol{u}_S$ vector is the direction of the transverse exciting dipole, typically either $\boldsymbol{u}_x$ or $\boldsymbol{u}_y$. The $r_{iB}$ are the impedances of the bottom cover transformed up to the bottom of the subject layer by the cascade of waveguides formed by each intervening layer and their surrounding conducting sidewalls, normalized by multiplying by each waveguide characteristic admittance, (9) or (10). Likewise, the $r_{iT}$ are the corresponding transformation of the top cover down to the top of the surface of the subject layer.

The Green's function for the $z$-directed electric field due to a transverse $\boldsymbol{u}_S$-directed exciting infinitesimal dipole is summed over only TM modes as TE modes have no $z$-directed electric field

$$\boldsymbol{G}_{tz} = -\sum_{\text{TM}} \frac{g_{T2}(z)g_B(z')\left[\boldsymbol{u}_S \cdot \boldsymbol{e}_{\text{it}}(x', y')\right]}{Y_i D}\boldsymbol{e}_{iz}^{\text{TM}}(x, y), \quad z \geq z' \tag{28}$$

$$\boldsymbol{G}_{tz} = \sum_{\text{TM}} \frac{g_T(z')g_{B2}(z)\left[\boldsymbol{u}_S \cdot \boldsymbol{e}_{\text{it}}(x', y')\right]}{Y_i D}\boldsymbol{e}_{iz}^{\text{TM}}(x, y), \quad z \leq z' \tag{29}$$

$$g_{B2}(u) = \cos(k_{iz}u) - r_{iB}\sin(k_{iz}u) \tag{30}$$
$$g_{T2}(u) = \cos(k_{iz}(h-u)) - r_{iT}\sin(k_{iz}(h-u)). \tag{31}$$

The Green's function for $z$-directed electric field due to a $z$-directed infinitesimal dipole likewise includes only TM modes as TE modes have no $z$-directed electric field. The Green's function is derived by considering a three-layer medium with identical constitutive parameters in all three layers. With a uniform $z$-directed filament of current extending across the thickness of the middle layer [14], we take the limit as the thickness of the middle layer goes to zero

$$\boldsymbol{G}_{zz} = \sum_{\text{TM}} \frac{k_z N_3 g_{T2}(z)g_{B2}(z')g_3(x', y')}{Y_i D}\boldsymbol{e}_{iz}^{\text{TM}}(x, y), \quad z \geq z' \tag{32}$$

$$\boldsymbol{G}_{zz} = -\sum_{\text{TM}} \frac{N_3 g_3(x', y')}{Y_i}\left\{1 - \frac{k^2}{k_c^2}\right\}\boldsymbol{e}_{iz}^{\text{TM}}(x, y), \quad z = z' \tag{33}$$

$$\boldsymbol{G}_{zz} = \sum_{\text{TM}} \frac{k_z N_3 g_{T2}(z')g_{B2}(z)g_3(x', y')}{Y_i D}\boldsymbol{e}_{iz}^{\text{TM}}(x, y), \quad z \leq z'. \tag{34}$$

Note that the Green's function for $z$-directed electric field generated by $z$-directed current has a discontinuity at $z = z'$. We see a reciprocity-based symmetry in (22)–(34).

## VI. Volume Subsection Fields

Fields surrounding a subsection require these Fourier-related constants

$$C_{i\text{VIA}}(x, y) = F_R(\Delta x)F_R(\Delta y)N_3 g_3(x, y) \tag{35}$$
$$C_{iRFX}(x, y) = F_T(\Delta x)F_R(\Delta y)[\boldsymbol{e}_{\text{it}}(x, y) \cdot \boldsymbol{u}_x] \tag{36}$$
$$C_{i\text{RFY}}(x, y) = F_R(\Delta x)F_T(\Delta y)\left[\boldsymbol{e}_{\text{it}}(x, y) \cdot \boldsymbol{u}_y\right] \tag{37}$$
$$F_R(\Delta x) = 2\sin(k_x \Delta x)/k_x, \quad k_x \neq 0 \tag{38}$$
$$F_R(\Delta x) = \Delta x, \quad k_x = 0 \tag{39}$$
$$F_T(\Delta x) = (1 - \cos(k_x \Delta x))/\Delta x k_x^2, \quad k_x \neq 0 \tag{40}$$
$$F_T(\Delta x) = 2\Delta x, \quad k_x = 0. \tag{41}$$

The electric field surrounding a volume rooftop centered at $(x_0, y_0)$ is determined by multiplying the Green's function by the volume rooftop basis function and performing an integration over the entire $(x', y', z')$ volume. The volume rooftop electric fields

$$\boldsymbol{E}_{t\mathrm{VRF}} = \sum_i \frac{C_{iS}(x_0, y_0)}{Y_i k_{iz}} \left(1 - \frac{g_T(z) + g_B(z)}{D}\right) \boldsymbol{e}_{\mathrm{it}}(x, y) \quad (42)$$

$$\boldsymbol{E}_{z\mathrm{VRF}} = -\sum_{\mathrm{TM}} \frac{C_{iS}(x_0, y_0) N_3 g_3(x, y)}{Y_i k_{iz}} \left(\frac{g_{T2}(z) g_{B2}(z)}{D}\right) \boldsymbol{u}_z \quad (43)$$

derive from (22) to (23) and from (28) to (29). The $C_{iS}$ are $C_{iRFX}$ for $x$-directed rooftops and $C_{i\mathrm{RFY}}$ for $y$-directed rooftops.

The electric field surrounding a uniform via centered at $(x_0, y_0)$ that occupies the entire thickness of the layer is determined by multiplying the Green's function by the volume uniform via basis function and performing an integration over the entire $(x', y', z')$ volume. The electric fields

$$\boldsymbol{E}_{t\mathrm{UV}} = \sum_{\mathrm{TM}} \frac{C_{i\mathrm{VIA}}(x_0, y_0)}{Y_i} \left(\frac{g_{t\mathrm{UV}}}{D}\right) \boldsymbol{e}_{\mathrm{it}}^{\mathrm{TM}}(x, y) \quad (44)$$

$$g_{t\mathrm{UV}} = r_{iT} g_B(z) - r_{iB} g_T(z) \quad (45)$$

$$\boldsymbol{E}_{z\mathrm{UV}} = \sum_{\mathrm{TM}} \frac{C_{i\mathrm{VIA}}(x_0, y_0) N_3 g_3(x, y)}{Y_i} \left\{\frac{k^2}{k_c^2} - \frac{g_{z\mathrm{UV}}}{D}\right\} \boldsymbol{u}_z \quad (46)$$

$$g_{z\mathrm{UV}} = r_{iT} g_{B2}(z) + r_{iB} g_{T2}(z) \quad (47)$$

derive from (28) to (29) and from (32) to (34).

The electric field surrounding an up-tapered via centered at $(x_0, y_0)$ and occupying the entire thickness of the layer is determined by multiplying the Green's function by the volume tapered via basis function and performing an integration over the entire $(x', y', z')$ volume. The electric fields

$$\boldsymbol{E}_{t\mathrm{TV}} = \sum_{\mathrm{TM}} \frac{C_{i\mathrm{VIA}}(x_0, y_0)}{Y_i k_{iz} h} \left(1 - \frac{g_{t\mathrm{TV}}}{D}\right) \boldsymbol{e}_{\mathrm{it}}^{\mathrm{TM}}(x, y) \quad (48)$$

$$g_{t\mathrm{TV}} = (1 - r_{iT} k_{iz} h) g_B(z) - g_T(z) \quad (49)$$

$$\boldsymbol{E}_{z\mathrm{TV}} = \sum_{\mathrm{TM}} \frac{C_{i\mathrm{VIA}}(x_0, y_0) N_3 g_3(x, y)}{Y_i h} \left(\frac{g_{z\mathrm{TV}}}{D} + k_{iz} z \frac{k^2}{k_c^2}\right) \boldsymbol{u}_z \quad (50)$$

$$g_{z\mathrm{TV}} = (1 - r_{iT} k_{iz} h) g_{B2}(z) - g_{T2}(z) \quad (51)$$

derive from (28) to (29) and from (32) to (34).

## VII. Reaction Integrals

For a Galerkin implementation of the method of moments, we multiply the source subsection electric field by the field subsection basis function and integrate over the entire $(x, y, z)$ volume. For a source volume rooftop centered at $(x_0, y_0)$ and a field volume rooftop at $(x_1, y_1)$ with both occupying the entire thickness of the layer, we use the electric field of (42) yielding

$$S_{\mathrm{VRFtoVRF}} = \sum_i \frac{C_S(x_0, y_0) C_F(x_1, y_1)}{Y_i k_{iz}^2} \left(k_{iz} h - \frac{g_{S1}}{D}\right) \quad (52)$$

$$g_{S1} = 2 - g_{B2}(h) - g_{T2}(0) \quad (53)$$

where $C_S$ and $C_F$ are the source and field subsection Fourier coefficients $C_{iRFX}$ or $C_{i\mathrm{RFY}}$, respectively, (36) or (37).

Multiplying the electric field due to the source basis function of interest, (42)–(51), by the desired field subsection basis function (and by invoking reciprocity as needed), the desired method of moments reaction integrals of a tapered via to a surface current $x$-directed rooftop (located at the bottom of the subject dielectric layer), to a volume current $x$-directed rooftop, to a uniform via, and to another tapered via are

$$S_{\mathrm{TV\,to\,RFX}} = \sum \frac{C_{\mathrm{VIA}}(x_0, y_0) C_{\mathrm{RFX}}(x_1, y_1)}{Y_i k_{iz} h} \left(1 - \frac{g_{S2}}{D}\right) \quad (54)$$

$$g_{S2} = g_T(0) + r_{iB}(1 - r_{iT} k_{iz} h) \quad (55)$$

$$S_{\mathrm{TV\,to\,VRFX}} = \sum \frac{C_{\mathrm{VIA}}(x_0, y_0) C_{\mathrm{RFX}}(x_1, y_1)}{Y_i k_{iz}^2 h} \left(k_{iz} h - \frac{g_{S3}}{D}\right) \quad (56)$$

$$g_{S3} = 2 - r_{iT} k_{iz} h + (r_{iT} k_{iz} h - 1) g_{B2}(h) - g_{T2}(0) \quad (57)$$

$$S_{\mathrm{TV\,to\,UV}} = \sum \frac{C_{\mathrm{VIA}}(x_0, y_0) C_{\mathrm{VIA}}(x_1, y_1)}{Y_i} \left(\frac{g_{S4}}{D} + \frac{k^2}{2k_c^2} k_{iz} h\right) \quad (58)$$

$$g_{S4} = \left(\frac{r_{iT} - r_{iB}}{k_{iz} h} + r_{iT} r_{iB}\right)(1 - \cos(k_{iz} h)) - r_{iT} \sin(k_{iz} h) \quad (59)$$

$$S_{\mathrm{TV\,to\,TV}} = \sum \frac{C_{\mathrm{VIA}}(x_0, y_0) C_{\mathrm{VIA}}(x_1, y_1)}{Y_i} \left(\frac{g_{S5}}{D} + \frac{k^2}{3k_c^2} k_{iz} h\right) \quad (60)$$

$$g_{S5} = \frac{(1 - r_{iT} k_{iz} h)(k_{iz} h g_B(h) + g_{B2}(h) - 2) + g_{T2}(0)}{k_{iz}^2 h^2}. \quad (61)$$

Additional reaction integrals for uniform vias are

$$S_{\mathrm{UV\,to\,RFF}} = \sum \frac{C_{\mathrm{VIA}}(x_0, y_0) C_{\mathrm{RFF}}(x_1, y_1)}{Y_i} \left(\frac{g_{S6}}{D}\right) \quad (62)$$

$$g_{S6} = r_{iB}(r_{iT} - g_T(0)) \quad (63)$$

$$S_{\mathrm{UV\,to\,VRFF}} = \sum \frac{C_{\mathrm{VIA}}(x_0, y_0) C_{\mathrm{RFF}}(x_1, y_1)}{Y_i k_{iz}} \left(\frac{g_{S7}}{D}\right) \quad (64)$$

$$g_{S7} = (r_{iT} - r_{iB})(1 - cos(k_{iz} h)) \quad (65)$$

$$S_{\mathrm{UV\,to\,UV}} = \sum \frac{C_{\mathrm{VIA}}(x_0, y_0) C_{\mathrm{VIA}}(x_1, y_1)}{Y_i} \left(\frac{g_{S8}}{D} + \frac{k^2}{k_c^2} k_{iz} h\right) \quad (66)$$

$$g_{S8} = 2 r_{iT} r_{iB} - r_{iT} g_B(h) - r_{iB} g_T(0). \quad (67)$$

Subscript "RFF" is replaced by "RFX" or "RFY" as desired. Reaction integrals between surface rooftops are listed in [3].

This technique meshes only the embedded structure, where the structure is considered everything that is different from the embedding layered media. The layered media is not meshed because its effect is included to full numerical precision within the reaction integrals listed above. In practice, the embedding media can have hundreds, or even over 1000 layers with extreme ranges of thicknesses and constitutive parameters (both real and complex) with little impact on analysis speed. For a wide range of problems, this can result in a considerably faster analysis as compared to the various techniques that require meshing the entire volume.

## VIII. Loss

With regards to Ohmic loss, the method of moments reaction integral from a source subsection $S$ to a field subsection, $F$, is

$$S_{S\,\text{to}\,F} = \int_V \boldsymbol{E}_S \cdot \boldsymbol{J}_F dV = \int_V \frac{\boldsymbol{J}_S \cdot \boldsymbol{J}_F}{\sigma} dV. \tag{68}$$

Basis function current $\boldsymbol{J}_S$ on the source subsection generates an electric field $\boldsymbol{E}_S$ due to bulk conductivity $\sigma$ by Ohm's Law. This electric field is dotted with the field subsection basis function $\boldsymbol{J}_F$ and integrated over the entire volume to yield the desired Galerkin reaction integral. If the source and field subsection do not physically overlap or if their respective currents are orthogonal, the above integral is zero. In addition, $\sigma$ can in general be complex. This is useful in modeling, for example, kinetic inductance (common in superconductors) or for modeling small intra-layer volumes with different dielectric constants by invoking polarization current.

For volume rooftops (both $x$- and $y$-directed), the Ohmic self-coupling is

$$S_{\text{VRFtoSelf}} = \frac{8\Delta x \Delta y h}{3\sigma}. \tag{69}$$

For adjacent identically directed volume rooftop subsections, with each one overlapping half of the other, the adjacent Ohmic coupling is

$$S_{\text{VRFtoAdj}} = \frac{2\Delta x \Delta y h}{3\sigma}. \tag{70}$$

There is no Ohmic coupling between $x$- and $y$-directed volume rooftops that overlap because their currents are orthogonal and the dot product in (68) is zero.

Since the current is the same everywhere in a uniform via, the self-coupling is the volume of the via divided by the bulk conductivity

$$S_{\text{UV to Self}} = \frac{4\Delta x \Delta y h}{\sigma}. \tag{71}$$

The current in a tapered via varies linearly along the length, giving us

$$S_{\text{TV to Self}} = \frac{4\Delta x \Delta y h}{3\sigma}. \tag{72}$$

A tapered via and a uniform via occupying the same via block yields

$$S_{\text{TV to UV}} = \frac{2\Delta x \Delta y h}{\sigma}. \tag{73}$$

All other volume subsection Ohmic couplings are zero.

## IX. Validation

Since the horizontal volume rooftop subsections have already been validated [8], we select a thick horizontally oriented coupled line bend as the benchmark, Fig. 6 (left). All dielectric layers are set to free space. The geometry is such that we can rotate the circuit 90° and have the identical physical geometry, Fig. 6 (right). The rotated geometry requires analysis of two via stacks, each similar to the stack in Fig. 5. The figures are to scale, with box size 290-$\mu$m cubed, and with lines having a 10-$\mu$m square cross section with a 10-$\mu$m gap.

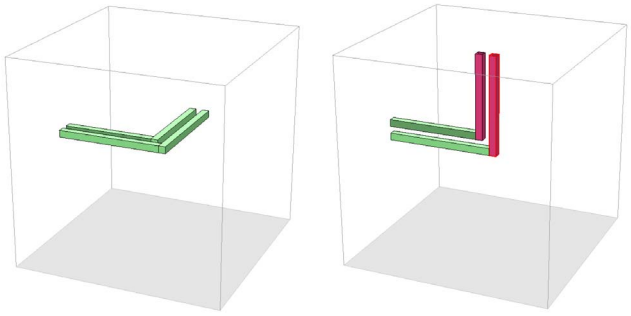

Fig. 6. Coupled line bend on the right is modeled using the previously validated horizontal volume rooftop subsections. The geometry is selected so that it can be rotated 90° and the circuit is physically identical. However, the vertical portion (red) of the rotated circuit (right) must be analyzed using a superposition of both tapered and uniform vias in each via block.

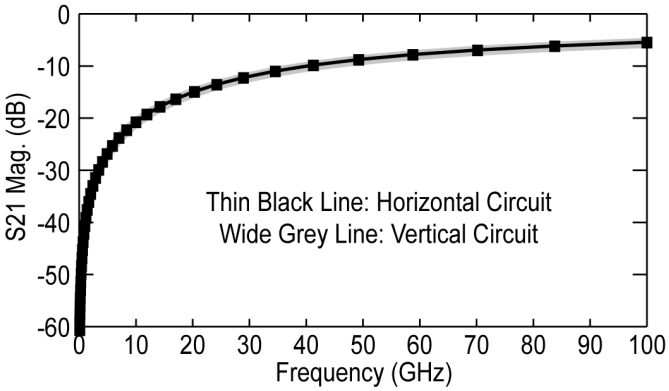


Fig. 7. Plot of $S_{21}$ magnitude (dB) for both circuits of Fig. 6 shows identical results (the two curves exactly overlap), thus validating both the tapered and uniform via theory.

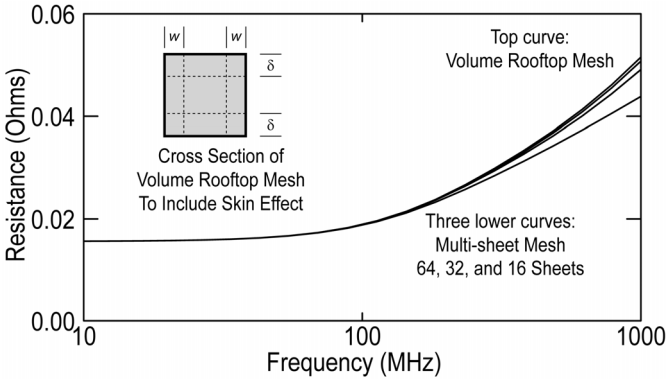


Fig. 8. Validation of the volume subsection loss model uses a simple through line modeled using both volume rooftop meshing and the already validated multisheet model. As the number of sheets increases, the multisheet model converges to the much faster three-layer volume mesh model.

Ports 1 and 2 are on the left and the other two ends are shorted to the adjacent sidewall or cover.

Fig. 7 shows $S_{21}$ magnitude (dB) for both circuits. Correct tapered and uniform via theory is required for the response of these two circuits to be identical, and that is the case. The agreement is so good that the two curves appear exactly one on top of the other.

Fig. 8 shows validation of the loss model using a stripline of 25 $\mu$m square $\times$400 $\mu$m long with 187.5 $\mu$m through the

air above and below. Metal conductivity is $4.09 \times 10^7$ S/m. We see that the multisheet model converges to the volume rooftop meshing. The volume rooftop mesh uses 3861 subsections while the converged (64 sheet) multisheet model uses 18 525 subsections. For this case, this makes the volume subsection model about $5^3 = 125$ times faster than the converged multisheet model. Analysis error is estimated by observing the nature and magnitude of the convergence here and in other validations presented below.

For accurate loss analysis using volume rooftop subsections, a meshing that allows modeling of the actual current distribution must be used. If the conductor has either thickness or width or both cross-sectional dimensions less than around two skin depths, the volume subsection cross section can be the same as the transmission line. This results in the fastest possible analysis. If the cross-sectional dimensions are larger, then volume subsections should be selected so that the outer layers (top, bottom, and sides) are roughly one skin depth thick, as shown in the inset of Fig. 8. This allows for accurate modeling of not only skin depth, but also line inductance and capacitance. Slightly higher accuracy is realized if the skin effect volume is meshed even more finely.

The insets of Figs. 8 and 9 illustrate this meshing. Either two or three layers of volume subsections are used. When the line is less than two skin depths thick, the top and bottom layers occupy the entire volume of the line, and there is no middle layer. When the line is greater than two skin depths thick, the top and bottom layers are each one skin depth ($\delta$) thick with the middle layer occupying the remaining volume.

The horizontal thickness of the sidewalls is set by the subsection width ($w = 2\Delta y$ for $x$-directed lines), and, for Fig. 8, this is 0.4 $\mu$m so that the volume meshing results are highly converged. This is important only if the sides of the middle layer carry a significant portion of the total current. When the line thickness and width both significantly exceed two skin depths, there is little current on the interior of the line and meshing for this interior region may be left out yielding a hollow tube model. This allows a faster analysis with slightly reduced accuracy.

Fig. 9 shows measured data (from [5], courtesy of M. Ashman, A. Durham, and B. Weaver, then of M/A-COM) for a microstrip line 51 $\mu$m wide on 100 $\mu$m thick GaAs. The line is 6888 $\mu$m long, 135 times longer than it is wide. Four lines were measured with both $S_{21}$ and $S_{12}$ magnitude dB of all four lines averaged together. To give an indication of measurement uncertainty, twice the sample standard deviation is plotted, which indicates an approximately 95% confidence interval.

We see the lower frequency results all cluster exceptionally close to the measured data, indicating that the subsection size is of little concern for frequencies less than 3 GHz, for which the line is six skin depths thick or less. High-frequency results show small error, which decreases as the subsection width becomes smaller. In the region from 4 to 12 GHz, the analysis converges nicely, however, it appears to be converging to a value slightly below the measured data. A "perfect" measurement would be smooth. However, there is a clear, all be it tiny, step up from 3.5 to 4 GHz. We suspect that

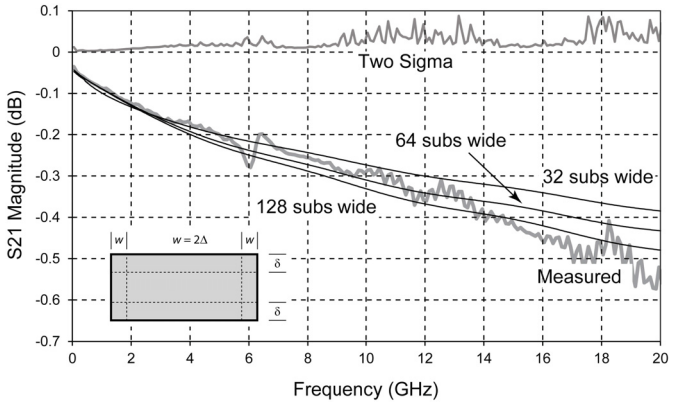


Fig. 9. Measured and calculated results for a 9 $\mu$m thick by 51 $\mu$m wide $\times$6888 $\mu$m long line. This line is 15 skin depths thick at 20 GHz. Subsection width, $w$, is the linewidth divided by the number of subsections across the width of the line. Three layers of volume rooftop subsections are used with the top and bottom layers one skin depth, $\delta$, thick. Sides are one subsection width wide, $w = 2\Delta y$ for $x$-directed lines. Highest accuracy is seen when they are about one skin depth at the highest frequency. Measured data is from [5] with estimated measurement error indicated by the top, "Two Sigma" curve (see text).

the apparent resonance at 8 GHz might be influencing the measured data from 4 to 12 GHz. The measurement error due to this resonance is not included in the error analysis. The resonance might be in the test fixture, but it might also be an artifact of calibration. We have not explored these hypotheses further. As with all models, narrow subsection width is needed only near the outside edges of the line. Wider subsections are used in the interior of the line.

The conductivity of the metal for this line is $\sigma = 3.45 \times 10^7$ S/m ($\rho = 2.90$ $\mu\Omega$-cm). This 9-$\mu$m-thick line is two skin depths thick at 0.36 GHz, three skin depths thick at 0.8 GHz, and 15 skin depths thick at 20 GHz, the highest frequency measured. The cell size ($2\Delta y$ for $x$-directed lines) for the 32 cell wide meshing is 51 / 32 = 1.6 $\mu$m, which is one skin depth wide at 2.8 GHz. The 64 cell wide meshing cell size is 0.8 $\mu$m, which is one skin depth wide at 11.5 GHz. The 128 cell wide meshing cell size is 0.4 $\mu$m, which is one skin depth wide at 46 GHz.

With these results we conclude that the meshing models described above converge to the correct result as the meshing is refined, at least to within measurement error. In addition, we also observe that in all cases, the error tends to be small with respect to a wide range of typical design requirements and small compared to measurement error.

For accurate analysis of lossless thick conductors, which have zero skin depth, the top and bottom layers can be made as thin as desired, or even exactly zero thickness by using surface current rooftops. The thickness of the side meshing is determined by the subsection width ($2\Delta y$ for a $x$-directed subsection), which should be about equal to the skin depth or smaller. For the lossless case, simply make the subsection width as small as reasonably practical. The loss evaluates to zero no matter the subsection width.

We have also performed substantial validation versus measurement for a wide range of SiRFIC components from several commercial sources. All of these results are considered proprietary by their sources.

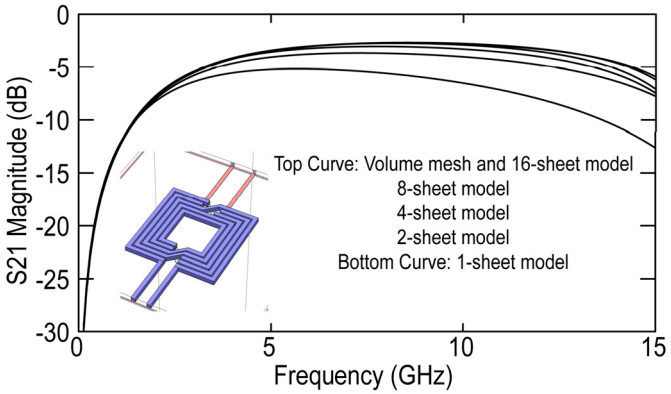


Fig. 10. Plot of $S_{21}$ magnitude (dB) for a rectangular spiral transformer on silicon. The 16-sheet model result is indistinguishable from the volume mesh results (top curve). The lower four curves show the 8-, 4-, 2-, and 1-sheet model results. The rectangular transformer is shown and is to scale. Input and output ports are differential so that ground return path is not an issue.

In order to show results comparable to a typical radio frequency integrated circuit (RFIC) validation, we take a public domain SiRFIC circuit from the examples provided with Sonnet Suites [11]. This example, "Rectangular Transformer," uses 10-$\mu$m wide lines separated by 4-$\mu$m gaps. To make the example especially sensitive to metal thickness error, we increased the metal thickness from 2 to 12 $\mu$m. The thickness of the embedding dielectric layer was also increased to 12 $\mu$m and the cell size used to mesh was increased to 2 $\mu$m. The top metal is on top of multiple layers of passivation, totaling about 7 $\mu$m in thickness. This in turn is on top of 725 $\mu$m of silicon. Differential ports are used on input and output. Otherwise, specific information on the ground return path (in a ground cage or other embedding circuit) would be needed.

We performed a convergence analysis for this circuit using the multisheet model starting with one sheet and going to 16 sheets. We compared these results with the three-layer volume mesh result. Fig. 10 shows both an image of the circuit and the results.

The 16-sheet model and the volume mesh results are indistinguishable when plotted at this scale. We see that the multisheet model converges to the three-layer volume mesh model extremely well. The 1-sheet model (bottom curve) uses 3188 subsections, 86 Mbytes of memory and needs only 4 s per frequency, however that result shows considerable difference from the converged result. The 16-sheet model requires 31 815 subsections, 7750 Mbytes of memory, and 35 m 27 s per frequency. The three-layer volume mesh model uses 9169 subsections, 652 Mbytes of memory, and 1 m 11 s per frequency with results essentially identical to the much slower 16-sheet model. This represents a 30 times improvement in speed for the same level of accuracy for this structure.

For all results shown here, the smallest subsection size is set by the cell size, $2\Delta x \times 2\Delta y$. Actual subsections (each using one moment matrix row/column per subsection) are formed from multiple cells. Subsections are automatically made narrow (e.g., one cell wide) at metal edges (e.g., one cell wide), to accurately represent the edge singularity, and are multiple cells wide on the interior. The same horizontal meshing is used for both the multisheet model and the volume mesh model.

## X. Conclusion

These results enable, for the first time, a complete *volume current*-based method of moments analysis of 3-D structures embedded in shielded multilayered media. In addition, the volume rooftops combined with the tapered and uniform via basis functions form the key elements required for analysis of completely arbitrary 3-D structures embedded in shielded layered media. The method of moments reaction integrals for both surface and volume meshings used here are evaluated to full numerical precision using a 2-D FFT and typically have little or no impact on analysis time for a given number of subsections. Volume rooftop subsections allow planar structures that use thick conductors to be accurately modeled with far fewer subsections. This in turn results in several orders of magnitude faster analysis for accurate analysis of such circuits. Looking to the future, these new volume rooftop subsections, including the equivalent of vertical volume rooftop subsections (which are enabled by the tapered and uniform volume vias described above) make method of moments analysis of arbitrary 3-D structures embedded in layered media possible and will become fully practical upon realization of appropriate user interfaces.

## References

[1] R. F. Harrington, *Field Computation by Moment Methods*. New York, NY, USA: Macmillan, 1968.

[2] K. A. Michalski and J. R. Mosig, "Multilayered media Green's functions in integral equation formulations," *IEEE Trans. Antennas Propag.*, vol. 45, no. 3, pp. 508–519, Mar. 1997.

[3] J. C. Rautio and R. F. Harrington, "An electromagnetic time-harmonic analysis of shielded microstrip circuits," *IEEE Trans. Microw. Theory Techn.*, vol. MTT-35, no. 8, pp. 726–730, Aug. 1987.

[4] A. A. Vyas, C. Zhou, and C. Y. Yang, "On-chip interconnect conductor materials for end-of-roadmap technology nodes," *IEEE Trans. Nanotechnol.*, vol. 17, no. 1, pp. 4–10, Jan. 2018.

[5] J. C. Rautio and V. Demir, "Microstrip conductor loss models for electromagnetic analysis," *IEEE Trans. Microw. Theory Techn.*, vol. 51, no. 3, pp. 915–921, Mar. 2003.

[6] S. J. Polychronopoulos and N. K. Uzunoglu, "Propagation and coupling properties of integrated optical waveguides—An integral equation formulation," *IEEE Trans. Microw. Theory Techn.*, vol. 44, no. 5, pp. 650–6451, May 1996.

[7] R. Gholami, S. Zheng, and V. Okhmatovski, "Overview of surface-volume-surface electric field integral equation formulations for 3-D composite metal-dielectric objects," in *Proc. 14th Eur. Conf. Antennas Propag. (EuCAP)*, Copenhagen, Denmark, Mar. 2020, pp. 1–4.

[8] A. Glisson and D. Wilton, "Simple and efficient numerical methods for problems of electromagnetic radiation and scattering from surfaces," *IEEE Trans. Antennas Propag.*, vol. AP-28, no. 5, pp. 593–603, Sep. 1980.

[9] J. C. Rautio and M. Thelen, "Volume rooftop basis functions in shielded layered media," in *Proc. IEEE Int. Conf. Numer. Electromag. Multiphys. Modeling Optim. (NEMO)*, Boston, MA, USA, May 2019, pp. 1–4.

[10] J. C. Rautio, "Virtual tool for designing planar circuits," U.S. Patent 62 848 234, May 15, 2019.

[11] Sonnet Software. Accessed: Nov. 2020. [Online]. Available: http://www.sonnetsoftware.com

[12] J. C. Rautio and M. A. Thelen, "A volume current based method of moments analysis of shielded planar 3-D circuits in layered media," in *IEEE MTT-S Int. Microw. Symp. Dig.*, Jun. 2020, pp. 146–149.

[13] N. Marcuvitz, *Waveguide Handbook*. London, U.K.: Peter Peregrinus, 1986.

[14] C. A. Balanis, *Advanced Engineering Electromagnetics*. New York, NY, USA: Wiley, 1989, p. 887.

**James C. Rautio** (Life Fellow, IEEE) received the B.S.E.E. degree from Cornell University, Ithaca, NY, USA, in 1978, the M.S. degree in systems engineering from the University of Pennsylvania, Philadelphia, PA, USA, in 1981, and the Ph.D. degree in electrical engineering from Syracuse University, Syracuse, NY, USA, in 1986, under the supervision of Dr. R. Harrington.

From 1978 to 1986, he was with General Electric, Syracuse, NY, USA, initially with the Valley Forge Space Division, then with the Syracuse Electronics Laboratory. During this time, he adeveloped microwave design and measurement software and designed microwave circuits on alumina and on GaAs. From 1986 to 1988, he was a Visiting Professor with Syracuse University Syracuse, NY, USA, and Cornell University. In 1988, he took Sonnet Software, Inc., North Syracuse, NY, USA, full time, a company he had founded in 1983. In 1995, Sonnet Software was listed on the Inc. 500 list of the fastest growing privately held U.S. companies, the only microwave software company ever to be so listed. Sonnet Software is currently the leading vendor of high accuracy 3-D planar high-frequency electromagnetic analysis software.

Dr. Rautio was the recipient of the 2001 IEEE Microwave Theory and Techniques Society (IEEE MTT-S) Microwave Application Award. He received the 2014 MTT Distinguished Service Award and the 2019 MTT Career Award. He was appointed as the MTT Distinguished Microwave Lecturer for 2005–2007 Lecturing on the life of J. C. Maxwell.

**Matthew A. Thelen** (Member, IEEE) received the B.S. degree in electrical engineering from Michigan Technological University, Houghton, MI, USA, in 1988, and the M.S. degree in electrical engineering from Syracuse University, Syracuse, NY, USA, in 1991.

From 1988 to 1995, he worked as an Engineer, with a focus on sonar sensor systems and signal processing, with the Aerospace Departments of General Electric Company, Syracuse, and Lockheed Martin Corporation, Syracuse. Since 1995, he has been a Senior Engineer with Sonnet Software, Inc., North Syracuse, NY, with responsibilities including research, development, and programming for high-frequency electromagnetic simulation EDA software.